# Effect of nitrogen on the electronic properties of ultrananocrystalline diamond thin films grown on quartz and diamond substrates

P. Achatz,[1] O. A. Williams,[2] P. Bruno,[3] D. M. Gruen,[3] J. A. Garrido,[1,*] and M. Stutzmann[1]
[1]*Walter Schottky Institut, Technische Universität München, Am Coulombwall, D-85748 Garching, Germany*
[2]*Institute for Materials Research, Universiteit Hasselt, Wetenschapspark 1, 3590 Diepenbeek, Belgium*
[3]*Materials Science Division, Argonne National Laboratory, Argonne, Illinois 60439, USA*

(Received 15 May 2006; published 25 October 2006)

The electronic transport properties of ultrananocrystalline diamond thin films grown from an argon-rich $Ar/CH_4$ microwave plasma have been investigated in the temperature range from 300 up to 700 K and as a function of nitrogen added to the gas phase (from 0 to 20%). The influence of nitrogen incorporation on the electronic transport properties of the ultrananocrystalline diamond films was examined by conductivity and Hall effect experiments. Electron spin resonance and electrically detected magnetic-resonance measurements complement the electronic transport study. In the case of films grown with a high nitrogen content in the gas phase, it was possible to perform Hall effect experiments, which showed n-type conductivity, with carrier concentrations up to $10^{20}$ $cm^{-3}$ and mobilities above 1 $cm^2/V\,s$ at room temperature. From the temperature dependence of the conductivity, we propose that electron transport via grain boundaries can explain the high conductivity (up to 150 $\Omega^{-1}$ $cm^{-1}$) of nitrogen containing ultrananocrystalline diamond films. The conduction mechanism in these films is explained by a transition from variable range-hopping transport in localized states near the Fermi level (in the case of low-conductivity films) to defect band conduction (in the case of high-conductivity films). The results have been discussed using a hopping model which assumes an exponential distribution of the density of states near the Fermi level, in order to explain the temperature dependence of the conductivity in the temperature range from 300 up to 700 K. Electrically detected magnetic resonance confirms that the transport of the low-conductivity samples can be explained by hopping via carbon dangling bonds.

DOI: 10.1103/PhysRevB.74.155429 PACS number(s): 73.63.Bd, 72.20.Ee

## I. INTRODUCTION

The influence of nitrogen incorporation on the bonding structure of ultrananocrystalline diamond was recently examined by Birrell *et al.*.[1] Nitrogen incorporation leads to an increase of the amount of $sp^2$-bonded carbon, whereas the grains remain $sp^3$-bonded. This supports the hypothesis of grain boundary conduction[2] to explain the high conductivity in "nitrogen-doped" samples. The n-type nature of the conductivity was confirmed by Hall and Seebeck effect measurements.[3] Recent work has used a model combining band and hopping transport to account for the conductivity mechanism in nitrogen-doped nanocrystalline diamond in the low temperature range (4.2 to 300 K), on the basis of the electronic structure of amorphous carbon.[4]

In this paper, the electronic properties of ultrananocrystalline diamond films have been studied in the temperature range 300–700 K for a better understanding of the electronic band structure and the influence of nitrogen incorporation. Electron spin resonance (ESR) and electrically detected magnetic resonance (EDMR) measurements complement the study of the temperature dependence of the conductivity and of the Hall coefficient.

## II. EXPERIMENTAL

Ultrananocrystalline diamond films were grown in a microwave plasma chemical vapor deposition (MPECVD) process from an argon-rich $Ar/N_2/CH_4$ gas phase. The films investigated here were grown either on quartz substrates (suitable for transport measurements) or on 100-oriented type Ib diamond. The quartz substrates were prepared by mechanical polishing with fine diamond powder, in order to provide a high density of nucleation sites for film growth. The $CH_4$ flow rate was kept constant at 1.4 standard cubic centimeter per min (SCCM), while the flow rate of $N_2$ and Ar was varied to maintain a 100 SCCM total flow rate. The substrate temperature was maintained at 800 °C, while the total pressure and input power were 100 Torr and 1200 W, respectively. $N_2$ [vol. %] refers to the amount of nitrogen in the gas phase. Five different series of samples grown by $Ar/CH_4$ MPECVD were studied. These series are designated by a capital letter *R* and distinguished furthermore by an additional letter, from *RA* to *RE*. Samples from series *RD* were grown on diamond substrates in the same run as samples from series *RB*, grown on quartz substrates, with 0, 10, 15, and 20% of nitrogen in the gas phase. Series *RB* represents a complement to the first series *RA* (0, 5, 7, 8, 9, and 10% nitrogen in the gas phase) for highly doped samples. The main difference of series *RC* (0, 5, 8, 10% nitrogen in the gas phase) with respect to the other series is a shorter growth time, as well as the use of a thinner quartz substrate. Series *RE* (grown on quartz) complements the other series, with 0 and 3% nitrogen in the gas phase.

The van der Pauw geometry has been used for the measurements of resistivities and Hall coefficients. Care was taken to measure in the ohmic range. The Hall effect was measured switching the magnetic field between +1.8 and −1.8 T. The temperature dependence of the Hall coefficient $R_H$ and the conductivity were examined at temperatures in the range 300–650 K. ESR spectra have been measured at room temperature with the $TE_{102}$ resonator of a X-band spec-

 ©2006 The American Physical Society

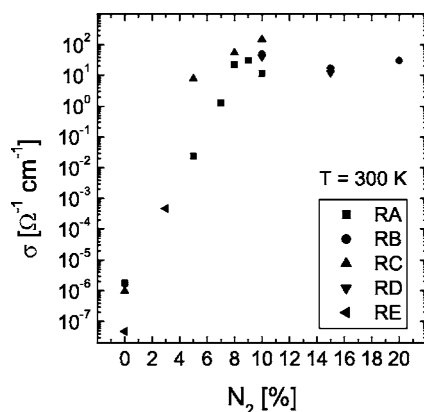


FIG. 1. Room-temperature conductivity versus nitrogen content in the gas phase for samples from the *R* series, grown from an argon-rich gas phase. The conductivity increases strongly with increasing nitrogen content.

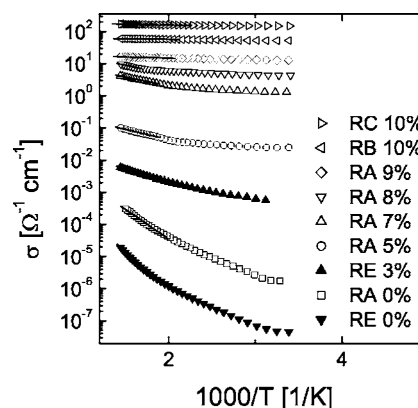


FIG. 2. Arrhenius plots of the conductivity $\sigma$ for samples of the *R* series, in the range 300 up to 700 K. Also shown is the linear fit in the high-temperature range, suggesting a change from variable-range hopping to simply activated conductivity.

trometer BRUKER ESP 300 operating at a microwave frequency of about 9.3 GHz. The magnetic field was modulated at 100 kHz and lock-in amplification was used to obtain a good signal to noise ratio.

## III. RESULTS AND DISCUSSION

In Fig. 1 the room-temperature conductivities $\sigma$ of all the samples grown from an argon-rich microwave plasma are plotted versus the nitrogen content in the gas phase during growth. The conductivity increases by almost nine orders of magnitude with increasing nitrogen content, and saturates for high nitrogen concentrations at a value close to $100\ \Omega^{-1}\ \mathrm{cm}^{-1}$. Bhattacharyya has reported a similar behavior of the conductivity with addition of nitrogen to the gas phase.[4] Hall measurements showed n-type conductivity in samples with nitrogen content higher than 5%, whereas in low-conductive samples no Hall effect was detected. The n-type nature of highly conductive ultrananocrystalline diamond was confirmed by Seebeck effect measurements.[3] Thus no sign anomaly of the Hall effect occurs, contrary to what is observed for several amorphous materials, e.g., amorphous silicon.

Figure 2 shows Arrhenius plots of the conductivity for ultrananocrystalline samples, from room temperature up to 700 K. A clear trend in the temperature dependence can be seen. The low-conductivity samples show a pronounced thermal activation. With increasing nitrogen content, the temperature dependence of the conductivity is reduced. The samples with the highest conductivity show a temperature-independent conductivity, i.e., quasimetallic behavior, in the investigated temperature range.

As discussed previously by Zapol *et al.*, the incorporation of nitrogen in ultrananocrystalline diamond is expected to change its electronic band structure by modifying the amount of $\pi$ and $\pi^*$ states in the band gap, and by introducing midgap states due to dangling bonds.[5] All these states are energetically centered around the Fermi level, while $\pi^*$ states due to distorted tetrahedrally bonded carbon atoms in the grain boundary are situated closer to the conduction band. Band tailing results in a reduction of the optical band gap of diamond. In the case of nitrogen-free ultrananocrystalline diamond these states are well localized.

Nitrogen is expected to be preferentially incorporated in the grain boundary region due to a lower substitutional energy.[5] Bond distortions are much easier achieved in the grain boundary region due to the local disorder, facilitating the incorporation of nitrogen in the grain boundaries. Thus, nitrogen is expected to increase the amount of $sp^2$-bonded carbon atoms, leading to a broadening of the $\pi$ and $\pi^*$ states,

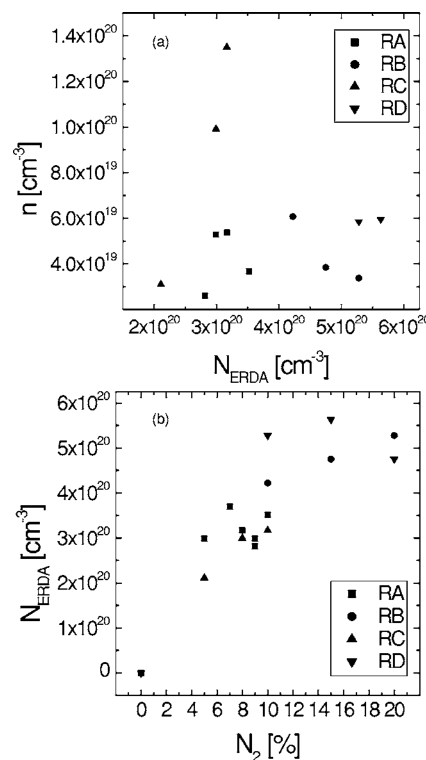


FIG. 3. (a) A comparison of the carrier concentration determined from Hall measurements with the concentration of nitrogen obtained from ERDA. (b) The concentration of nitrogen obtained from ERDA as a function of nitrogen in the gas phase.

TABLE I. Calculated parameters based on the Arrhenius plot of Fig. 2. The activation energy $E_a$ decreases with increasing conductivity. Highly conductive samples show simple thermal activation over the whole temperature range, the prefactor $\sigma_{\min}$ is used to estimate the inelastic scattering length $a$ using Eq. (2).

| Sample | $N_2$ [%] | $\sigma_{300\ K}$ [$\Omega^{-1}$ cm$^{-1}$] | $T$ [K] | $E_a$ [eV] | $\sigma_{\min}$ [$\Omega^{-1}$ cm$^{-1}$] | $a$ [Å] |
|---|---|---|---|---|---|---|
| *RE*0 | 0 | $5\times10^{-8}$ | 500–700 | 0.52 | | |
| *RA*0 | 0 | $2\times10^{-6}$ | 500–700 | 0.37 | | |
| *RE*3 | 3 | $5\times10^{-4}$ | 500–700 | 0.18 | | |
| *RA*5 | 5 | $2.4\times10^{-2}$ | 530–700 | 0.12 | | |
| *RA*7 | 7 | 1.3 | 550–700 | 0.11 | | |
| *RA*8 | 8 | 4.4 | 620–700 | 0.12 | | |
| *RA*9 | 9 | 13 | 300–700 | 0.015 | 21 | 34 |
| *RB*10 | 10 | 52 | 300–700 | 0.0078 | 69 | 11 |
| *RC*10 | 10 | 148 | 300–700 | 0.0086 | 197 | 3.7 |

as well as increasing delocalization of these levels. Thus, $\pi$ and $\pi^*$ bands are formed and the material becomes more and more graphitic with increasing nitrogen content. In pure diamond nitrogen acts as a deep donor: substitutional nitrogen forms a deep level 1.7 eV below the conduction band edge, and therefore its contribution to the conduction is negligible at room temperature.

Zapol *et al.* have suggested that the electrical transport in ultrananocrystalline diamond can be explained by a combination of thermally activated transport in extended states and hopping transport in localized states.[5] The transport of the low-conductivity samples is expected to be dominated by hopping conduction in defect states around the Fermi level. The main impact of nitrogen is the increasing of delocalization of the $\pi$ and $\pi^*$ bands, and the upward shift of the Fermi level towards the $\pi^*$ band. An enhancement of hopping conduction and thermal activation of carriers to the delocalized $\pi^*$ band accounts for the high conductivity in highly doped samples. The increasing graphitization of ultrananocrystalline diamond due to nitrogen incorporation can therefore explain the strong increase in conductivity seen in Fig. 1.

The results in Fig. 2 show that, while the highly conductive samples can be described by a single activated transport throughout the whole temperature range, low-conductivity samples show a transition in the activated behavior of the conductivity. A combination of variable range hopping in the low-temperature range and thermally activated conduction in the high-temperature range will be discussed below. The activation energies $E_a$ determined from the linear fit of the experimental results in the high-temperature regime are listed in Table I.

A decrease of the activation energy $E_a$ with increasing conductivity is observed. As already mentioned, nitrogen incorporation is expected to broaden the $\pi$ and $\pi^*$ bands. Additionally, the theoretical work of Zapol *et al.* has predicted that nitrogen incorporation results in an upward shift of the Fermi level towards the conduction band, and thus toward the $\pi^*$ band. The simple thermal activation of the conductivity observed in the high-temperature regime can therefore be explained by considering conduction in the extended states of a defect band. The lowering of the activation energy is in accordance with the upward shift of the Fermi level, which moves closer to the mobility edge of the impurity band. The increasing delocalization of the $\pi$ and $\pi^*$ states with nitrogen incorporation leads to quasimetallic behavior. The conductivity for disordered solids described by Mott[6] can be written as

$$\sigma(T) = \sigma_0 \exp\left[-\frac{(E_c - E_F)}{k_B T}\right]. \quad (1)$$

$E_c$ is the mobility edge, separating localized states from extended states. For disordered three-dimensional (3D) networks $\sigma_0$ is given by

$$\sigma_0 = \sigma_{\min} = \frac{0.03e^2}{\hbar a} \quad (2)$$

with $a$ the inelastic scattering length.[6] This value is known as the minimum metallic conductivity ($\sigma_{\min}$), and can be used to estimate the inelastic scattering length $a$, see Table I. For $a$=3 Å (as in metals) $\sigma_{\min}$ is about 200 $\Omega^{-1}$ cm$^{-1}$.

Only highly conductive samples with a large amount of nitrogen showed a measurable Hall effect. Low-conductivity samples showed no Hall signal, probably due to the low value of the carrier mobilities. All values of the Hall mobility are in the range from 1 to 7 cm$^2$ V$^{-1}$ s$^{-1}$ and remain approximately constant over the whole temperature range (from 300 up to 700 K).

The carrier concentration $n$ derived from the Hall effect experiments shows a weak temperature dependence, following the conductivity $\sigma$. Figure 3 compares the concentration of mobile carriers $n$ with the concentration $N_{ERDA}$ of nitrogen incorporated in the samples and obtained by elastic recoil detection analysis (ERDA). Both concentrations are normalized to the bulk volume and not to the (unknown) volume fraction of the grain boundary region. Except for series *RC* no clear trend with nitrogen incorporation can be observed. Increasing the amount of nitrogen in the gas phase above a certain value (between 5 and 10%) does not result in an increase of nitrogen incorporation in the films, which leads to the saturation of the conductivity shown in Fig. 1. The nitrogen concentration measured from ERDA is almost one order of magnitude larger than the Hall carrier concentration.

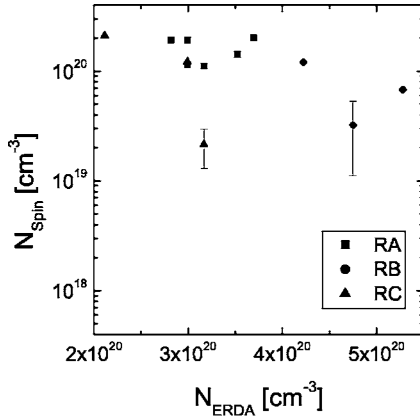


FIG. 4. Variation of the ESR spin density $N_{spin}$ with increasing nitrogen content obtained from ERDA measurements. A clear trend with nitrogen content cannot be observed.

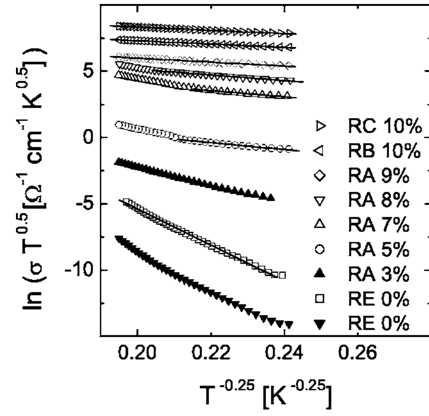


FIG. 5. Variation of $\sigma\sqrt{T}$ with $T^{-0.25}$ for the same set of samples of the $R$ series as in Fig. 2, in the temperature range 300–700 K. Also shown are the linear fits at low temperatures:

Figure 4 shows the spin density $N_{spin}$ determined from ESR measurements as a function of incorporated nitrogen. The analysis of ESR data is done assuming a Lorentzian lineshape of the ESR spectra. Samples marked with error bars in Fig. 4 showed different (very broad) lineshapes. In this case, a detailed lineshape analysis by numerical integration would be necessary to obtain the correct values of the spin density. The spin density, normalized to the bulk volume, is about $1\times10^{20}$ cm$^{-3}$, independent of nitrogen content. Assuming that the defect states are located at the grain boundaries, as expected from the preferential incorporation of nitrogen into the grain boundaries, the density increases to $3\times10^{21}$ cm$^{-3}$, resulting in an average distance $r_{db}$ of about 4.4 Å. All spectra have a g factor of about 2.0025, typical for carbon dangling bonds. These defect states are well-localized states energetically located in the band gap, and thus, the Fermi level is pinned by these states. Therefore, hopping transport via these states can be assumed for the low-conductivity samples, while other transport mechanisms have to be taken into account for the highly conductive samples. This is supported by EDMR measurements: the low-conductive sample $RA0$ showed a signal with $\Delta\sigma/\sigma \approx 10^{-7}$. The highly conductive sample $RB10$ showed no EDMR signal.

Hopping transport requires the existence of localized states at the Fermi level. There are several types of hopping conduction, such as nearest neighbor hopping (NNH) and variable-range hopping (VRH). Thermally activated hopping occurs if the density of states at the Fermi level $N(E_F)$ is finite. Mott *et al.* have suggested that the required thermal activation energy $\Delta E$ decreases with the hopping distance $R_H$ between two sites, while hopping over a large distance reduces the probability for tunneling.[6] The probability for a carrier to hop from an occupied to an unoccupied site, separated by a distance $R$, depends on the overlap of the wave functions of the two sites and their energy difference $\Delta E$. This probability $\Gamma$ is given by

$$\Gamma \propto \exp(-2\alpha R)\exp\left(-\frac{\Delta E}{k_B T}\right), \tag{3}$$

in which the first exponential term describes the tunneling process between the two localized states, with $\alpha$ the decay

TABLE II. Parameters $A=\ln \sigma^{00}_{c,\mathrm{Mott}}$ and $B=T^{0.25}_{0,3}$ [K$^{0.25}$] from the linear fit in Fig. 5 are used to calculate values of the prefactor $\sigma^{00}_{c,\mathrm{Mott}}$ [$\Omega^{-1}$ cm$^{-1}$ K$^{0.5}$], the density of states $N(E_F)$ [cm$^{-3}$ eV$^{-1}$], the localization length $\xi$, and the average hopping distance $R_H$ based on Mott's variable-range hopping using a constant density of states at the Fermi level. Note the unphysical values of some parameters.

| Sample | $T$ [K] | $T^{0.25}_{0,3}$ (±1) | $\sigma^{00}_{c,\mathrm{Mott}}$ | $N(E_F)$ | $\alpha^{-1}$ [Å] | $R_H$ [Å] |
|---|---|---|---|---|---|---|
| *RA*0 | 300–700 | 136 | $3\times10^{9}$ | $2\times10^{41}$ | $1\times10^{-7}$ | $2\times10^{-4}$ |
| *RC*0 | 300–700 | 137 | $4.4\times10^{9}$ | $7\times10^{41}$ | $1\times10^{-7}$ | $1\times10^{-4}$ |
| *RE*0 | 300–700 | 150 | $2\times10^{9}$ | $6\times10^{40}$ | $2\times10^{-7}$ | $3\times10^{-4}$ |
| *RE*3 | 300–700 | 62 | $3\times10^{4}$ | $4\times10^{25}$ | $7\times10^{-2}$ | 41 |
| *RA*5 | 300–440 | 26 | $2\times10^{2}$ | $3\times10^{18}$ | 51 | $1\times10^{4}$ |
| *RA*7 | 300–420 | 23 | $5\times10^{3}$ | $3\times10^{22}$ | 3 | 590 |
| *RA*8 | 300–560 | 21 | $1\times10^{4}$ | $4\times10^{23}$ | 1 | 260 |
| *RA*9 | 300–700 | 15 | $8\times10^{3}$ | $5\times10^{22}$ | 4 | 600 |
| *RB*10 | 300–700 | 13 | $2\times10^{4}$ | $4\times10^{23}$ | 3 | 300 |
| *RC*10 | 300–700 | 12 | $5\times10^{4}$ | $8\times10^{24}$ | 1 | 120 |

parameter of the localized wave function. $\xi=1/\alpha$ is also known as the localization length. One of the main assumptions of Mott was an energy-independent distribution of localized states near the Fermi level, i.e., a constant $N(E_F)$.[6] A general expression for the resulting hopping conductivity, valid for transport in any $d$-dimensional space, can be written as

$$\sigma_d(T) = \sigma_{d,VRH} \exp\left[ -\left( \frac{T_{0,d}}{T} \right)^{1/(d+1)} \right], \quad (4)$$

where

$$T_{0,d}^{1/(d+1)} = \frac{2(d+1)}{d} \left[ \frac{d}{2\Omega_{1,d}} \right]^{1/(d+1)} \left( \frac{\alpha^d}{k_B N(E_F)} \right)^{1/(d+1)}. \quad (5)$$

Here, $\Omega_{1,d}$ is the volume of a $d$-dimensional sphere with unit radius (for instance $4\pi/3$ for $d=3$). A similar expression is derived for the optimum hopping distance $R_H$

$$R_{H,d} = \left( \frac{d}{2\Omega_{1,d}} \right)^{1/(d+1)} \left( \frac{1}{N(E_F)\alpha k_B T} \right)^{1/(d+1)}. \quad (6)$$

According to Mott's assumption of a constant density of states at the Fermi level, the 3D variable-range hopping is characterized by

$$T_{0,3} = \left( \frac{512}{9\pi} \right) \left( \frac{\alpha^3}{k_B N(E_F)} \right) \quad (7)$$

and for the optimum hopping distance $R_H$

$$R_{H,3} = \left( \frac{9}{8\pi} \right)^{1/4} \left( \frac{1}{N(E_F)\alpha k_B T} \right)^{1/4}. \quad (8)$$

The prefactor $\sigma_{d,VRH}$ derived by Mott shows a weak temperature dependence according to

$$\sigma_{3,VRH} = \left( \frac{1}{32\pi} \right)^{1/2} e^2 \left( \frac{N(E_F)}{\alpha k_B T} \right)^{1/2} \nu_{\text{ph}} = \sigma_{c,\text{Mott}}^{00} T^{-1/2} \quad (9)$$

for $d=3$. $\nu_{\text{ph}}$ is a typical phonon frequency ($10^{12}$–$10^{13}$ s$^{-1}$) contributing to the thermal activation of the hopping process and $\sigma_{c,\text{Mott}}^{00}$ represents the temperature-independent prefactor. The index $c$ indicates that a constant density of states $N(E_F)$ at the Fermi level was assumed. Other methods for deriving similar expressions, assuming a constant density of states $N(E)=N(E_F)$, give different values of $T_{0,d}$ and $R_{H,d}$, but the dependence on the decay parameter $\alpha$ and the density of states $N(E_F)$ remains valid.[7]

Figure 5 shows a plot of the conductivity $\sigma$ according to 3D variable-range hopping, following Eq. (4), for the same set of samples of the $R$ series as in Fig. 2, in the temperature range 300 to 700 K. Variable-range hopping in 3D can account for the low-conductivity undoped sample $RA0$ in the whole temperature range, while for the samples $RA5$, $RA7$, and $RA8$ a clear deviation can be seen in the higher temperature range. The dimensionality of thehopping process remains unclear in our case. Mott has shown that the exponential dependence of the conductivity $[T^{-1/(d+1)}]$ is a pure consequence of the hopping-space dimensionality $d$. In the following we focus on 3D hopping.

The crossover to simply activated behavior in Fig. 5 occurs at relatively high temperatures (500–600 K). A proper fit was also possible for the highly conductive samples throughout the whole temperature range due to the weak dependence on temperature. From the fitting parameters $A = \ln \sigma_{c,\text{Mott}}^{00}$ and $B = T_{0,3}^{0.25}$, the values for the localization length $\xi$, the density of states $N(E_F)$ at the Fermi level, and the average hopping distance $R_H$ (at 300 K) based on Mott's variable-range hopping can be derived (see Table II). As can be seen in Table II, many of these parameters have unphysical values, and only the values for the higher conductive samples seem reasonable to some extent. Therefore, Mott's variable-range hopping does not seem to be the appropriate way to describe the temperature dependence of the conductivity $\sigma$ in these samples. Nevertheless, at lower temperatures a constant density of states (Mott) would suffice, since only those states very close to the band edge are operative.

A main assumption in Motts' variable-range hopping model is a constant density of states, $N(E_F)$, at the Fermi level. Variable-range hopping was recently revisited by Godet *et al.*,[7] who considered an ensemble of uncorrelated lo-

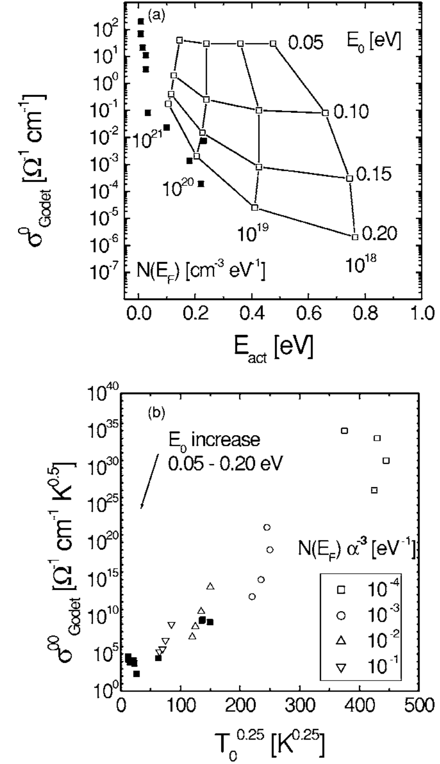


FIG. 6. (a) The correlation between computed prefactor $\sigma_{\text{Godet}}^{0}$ [$\Omega^{-1}$ cm$^{-1}$] and the activation energy $E_{\text{act}}$ [eV] derived from the hopping model in an exponential bandtail, using the disorder parameter $E_0$ and the density of states $N(E_F)$ as parameters. Data taken from Ref. 8. The localization length $\alpha^{-1}$ is kept fixed at 5 Å (Ref. 8). Black data points correspond to experimental values (seeTable III). (b) The relationship between the parameters $\sigma_{\text{Godet}}^{00}$ and $T_0$ derived from modeling of hopping conductivity in an exponential density of states. Data taken from Ref. 7. The disorder parameter $E_0$ varies in the range 0.05–0.20 eV and the localization parameter $N(E_F)$ $\alpha^{-3}$ in the range $10^{-4}$–$10^{-1}$ eV$^{-17}$. Black data points correspond to experimental values (see Table III).

TABLE III. Parameter $\sigma^{00}_{\text{Godet}}=\exp A$ [$\Omega^{-1}$ cm$^{-1}$ K$^{0.5}$] from the linear fit in Fig. 5, as well as calculated values for the localization parameter N $(E_F)$ $\alpha^{-3}$ [eV$^{-1}$] [see Eq. (11)]. The density of states N $(E_F)$ [cm$^{-3}$ eV$^{-1}$] at the Fermi level is estimated assuming a localization length $\alpha^{-1}$ of 5 Å. In addition, the prefactor $\sigma^{0}_{\text{Godet}}$ [$\Omega^{-1}$ cm$^{-1}$] and the activation energy $E_{\text{act}}$ [eV] of the Arrhenius plots is given, in the temperature range 300–400 K.

| Sample | $\sigma^{00}_{\text{Godet}}$ | N $(E_F)$ $\alpha^{-3}$ | N $(E_F)$ | $\sigma^{0}_{\text{Godet}}$ | $E_{\text{act}}$ |
|---|---|---|---|---|---|
| *RA*0 | $3\times10^{9}$ | $1\times10^{-2}$ | $8.4\times10^{19}$ | $7.5\times10^{-3}$ | 0.23 |
| *RC*0 | $4.4\times10^{9}$ | $1\times10^{-2}$ | $8\times10^{19}$ | $1.4\times10^{-3}$ | 0.18 |
| *RE*0 | $2\times10^{9}$ | $1\times10^{-2}$ | $5.7\times10^{19}$ | $1.9\times10^{-4}$ | 0.22 |
| *RE*3 | $3\times10^{4}$ | $2\times10^{-1}$ | $1.9\times10^{21}$ | $2.3\times10^{-2}$ | 0.1 |
| *RA*5 | $2\times10^{2}$ | 10 | $6\times10^{22}$ | $8.1\times10^{-2}$ | 0.03 |
| *RA*7 | $5\times10^{3}$ | 15 | $1\times10^{23}$ | 3.3 | 0.03 |
| *RA*8 | $1\times10^{4}$ | 20 | $1.4\times10^{23}$ | 11 | 0.03 |
| *RA*9 | $8\times10^{3}$ | 70 | $6\times10^{22}$ | 21 | 0.02 |
| *RB*10 | $2\times10^{4}$ | 140 | $1\times10^{24}$ | 70 | 0.008 |
| *RC*10 | $5\times10^{4}$ | 150 | $1\times10^{24}$ | 200 | 0.009 |

calized states randomly distributed in space. Furthermore, an exponential density of states (band tail) above the Fermi level was considered

$$\mathrm{N}(E) = \mathrm{N}(E_F)e^{(E-E_F/E_0)}, \qquad (10)$$

where $E_0$ is an electronic disorder parameter describing bandtailing due to disorder. For 3D hopping, the $T^{-0.25}$ power law is valid as in the case of Mott's variable-range hopping. The parameter $T_0^{0.25}$, representing the slope of the curves in Fig. 5, is related to the density of states $\mathrm{N}(E_F)$ at the Fermi level by the relationship

$$T_0 = 310\left(\frac{\alpha^3}{k_B \mathrm{N}(E_F)}\right) \qquad (11)$$

with a weak dependence on the disorder parameter $E_0$ [see Fig. 6(b)]. $\mathrm{N}(E_F)$ $\alpha^{-3}$ is known as the localization parameter. In Fig. 6(b), the relationship of the prefactor $\sigma^{00}_{\text{Godet}}$ and $T_0^{0.25}$ is displayed for several values of the localization parameter. A clear positive correlation between these two parameters can be seen, in contrast to the predictions of Mott's variable-range hopping.[7]

We observe that couples of parameters ($\sigma^{00}_{\text{Godet}}$, $T_0^{0.25}$) span a very wide range, typically $10^{3}$–$10^{35}$ $\Omega^{-1}$ cm$^{-1}$ K$^{0.5}$ for $\sigma^{00}_{\text{Godet}}$ and 60–450 K$^{0.25}$ for $T_0^{0.25}$.[8] This is in good accordance with the values obtained from the fitting for undoped low-conductivity samples from the *R* series, as can be seen in Table III. The localization parameter $\mathrm{N}(E_F)$ $\alpha^{-3}$ for these samples lies in the range 1 to $2\times10^{-2}$ eV$^{-1}$. This is consistent with the numerical modeling for hopping conductivity in an exponential density of states displayed in Fig. 6(b). The localization parameter $\mathrm{N}(E_F)$ $\alpha^{-3}$ for the numerical modeling lies in the range $10^{-4}$–$10^{-1}$ eV$^{-1}$, while corresponding values of the highly conductive samples (see Table III) are in the range $10^{1}$–$10^{2}$ eV$^{-1}$, indicating strong delocalization. An extrapolation towards high $\alpha^{-1}$ values can tentatively be performed, the situation corresponding to quasimetallic behavior, when the temperature dependence of the conductivity $\sigma$ vanishes.[9]

The temperature dependence of the conductivity $\sigma$ calculated from the hopping model in an exponential density of states is expected to follow the power law $T^{-0.25}$. Therefore, a curvatures in the Arrhenius plot of the conductivity will be observed, with an increase in the activation energy $E_{\text{act}}$ and the apparent conductivity prefactor $\sigma^{0}_{\text{Godet}}$ with increasing temperature.[8] Figure 6(a) shows the correlation of the computed prefactor $\sigma^{0}_{\text{Godet}}$, in the range 300–400 K, and the activation energy $E_{\text{act}}$, using $E_0$ and the density of states $\mathrm{N}(E_F)$ as parameters. The localization length $\alpha^{-1}$ is kept constant at 5 Å. Our experimental results for the low-conductivity samples agree quite well with the model, indicating values of the disorder parameter $E_0$ between 0.15–0.20 eV (see Table III). Furthermore, the model predicts reasonable values for the density of states $\mathrm{N}(E_F)$ at the Fermi level of about $1\times10^{20}$ cm$^{-3}$ eV$^{-1}$, in accordance with the density of dangling bonds. The assumed value for the localization length $\alpha^{-1}$ of 5 Å is comparable to the spatial distance of dangling bonds (4.5 Å) estimated from their density.

As one can see from Table III and Fig. 6, the values for the higher conductivity samples lie beyond the scope of this model.[7] As already mentioned, an extrapolation to higher $\xi$ values can be tentatively carried out. The values of the density of states at the Fermi level $\mathrm{N}(E_F)$, assuming a localization length $\alpha^{-1}$ of 5 Å, are too high. Reasonable values of the order $1\times10^{21}$ cm$^{-3}$ eV$^{-1}$ can be obtained for a localization length $\alpha^{-1}$ of 30 Å, suggesting a stronger delocalization in the highly conductive samples.

In addition, the carrier mobility can be estimated within this model.[10] Assuming a disorder parameter $E_0$ between 0.15–0.20 eV, a density of states at the Fermi level $\mathrm{N}(E_F)$ of about $1\times10^{20}$ cm$^{-3}$ eV$^{-1}$ and a localization length $\xi$ of 5 Å, values of the mobility $\mu_H$ in the range from $1\times10^{-5}$ to $1\times10^{-4}$ cm$^2$ V$^{-1}$ s$^{-1}$ are obtained for the low-conductive samples. These values are quite low and probably the reason why low-conductive samples showed no Hall signal. Furthermore, the temperature dependence of the hopping mobility is predicted within this model,[10] showing singly activated behavior with activation energies $E_\mu$ decreasing from

0.24 to 0.02 eV with increasing localization parameter $N(E_F)\ \alpha^{-3}$ from $1.5\times10^{-4}$ to $6.4\times10^{-1}$ eV$^{-1}$. Thus, the temperature dependence gets weaker with increasing delocalization. Extrapolation of the model to higher $\alpha^{-1}$ values[10] would lead to values of the hopping mobility $\mu_H$ in the range $1-10$ cm$^2$ V$^{-1}$ s$^{-1}$, quite independent of temperature. This is in accordance with the experimental mobility data for thehighly conductive samples.

## IV. CONCLUSION

The electronic transport properties of ultrananocrystalline diamond films grown from an argon-rich $Ar/CH_4$ microwave plasma have been studied in the temperature range from 300 up to 700 K, and the influence of nitrogen incorporation has been examined.

The conduction mechanism can be explained by a transition from hopping transport in localized states to impurity band conduction. The low-conductivity samples ($\sigma \approx 10^{-6}\ \Omega^{-1}$ cm$^{-1}$ at $T=300$ K) follow the $T^{-0.25}$ law for 3D hopping over the whole temperature range (300–700 K). However, we have shown that Mott variable-range hopping is not able to describe the temperature dependence of the conduction, leading to unreasonable values for the physical parameters deduced from the experimental results. A hopping model which assumes an exponential distribution of the density of states near the Fermi level has been applied instead.[7] The $T^{-0.25}$ power law only depends on the dimensionality of the hopping space of accessible states. An extrapolation of Godet's model can be used to account for the high conductivity in samples with a large amount of nitrogen, although the assumptions for the model are no longer valid. The conductivity of the samples increases by almost nine orders of magnitude with increasing nitrogen content, leading to a quasimetallic behavior for the highly conductive samples. Hall measurements confirm the n-type nature of the conductivity for the nitrogen containing samples, as well as nearly temperature-independent values for the Hall mobility (1 to 10 cm$^2$ V$^{-1}$ s$^{-1}$) in the case of highly conductive samples. Due to the weak temperature dependence of the conductivity for the highly conductive samples, a single activated conductivity with small activation energies of about 0.01 eV corresponding to impurity band conduction was found. The low-conductivity samples show a crossover from hopping to thermally activated conductivity at high temperatures. Furthermore, ESRand EDMR experiments indicate that the conductivity of the low-conductivity samples can be explained by hopping via dangling bond states. The activation energy of the conductivity decreases with increasing nitrogen content. Nitrogen, preferentially incorporated in the grain boundaries, is expected to increase the amount of $sp^2$-bonded carbon in the grain boundaries. The $sp^2$-bonded carbon atoms introduce localized $\pi$ and $\pi^*$ defect states in the band gap of diamond. Thus, nitrogen incorporation leads to an increasing delocalization of these states and to a broadening of the $\pi$ and $\pi^*$ defect bands. Together with a shift of the Fermi level towards the conduction band with increasing nitrogen content, this can count for the temperature dependence of the conductivity corresponding to $\pi^*$ impurity or defect band conduction.

## ACKNOWLEDGMENTS

We thank M. Brandt for his support and stimulating discussions on ESR and EDMR experiments. A. Bergmaier is acknowledged for performing ERDA measurements. This work has been partially supported by DRIVE (Diamond Research on Interfaces and Versatile Electronics) Marie Curie Research Training Network.

*Electronic address: garrido@wsi.tum.de

[1] J. Birrell, J. E. Gerbi, O. Auciello, J. M. Gibson, D. M. Gruen, and J. A. Carlisle, J. Appl. Phys. **93**, 5606 (2003).
[2] S. Bhattacharyya, O. Auciello, J. Birrell, J. A. Carlisle, L. A. Curtiss, A. N. Goyette, D. M. Gruen, A. R. Krauss, J. Schlueter, A. Sumant *et al.*, Appl. Phys. Lett. **79**, 1441 (2001).
[3] O. A. Williams, S. Curat, J. E. Gerbi, D. M. Gruen, and R. B. Jackman, Appl. Phys. Lett. **85**, 1680 (2004).
[4] S. Bhattacharyya, Phys. Rev. B **70**, 125412 (2004).
[5] P. Zapol, M. Sternberg, L. A. Curtiss, T. Frauenheim, and D. M. Gruen, Phys. Rev. B **65**, 045403 (2002).
[6] N. Mott, *Conduction in Non-Crystalline Materials* (Oxford Science Publications, New York, 1993), 2nd ed.
[7] C. Godet, J. Non-Cryst. Solids **299-302**, 333 (2002).
[8] C. Godet, Philos. Mag. B **81**, 205 (2001).
[9] C. Godet, Phys. Status Solidi B **231**, 499 (2002).
[10] C. Godet, Diamond Relat. Mater. **12**, 159 (2003).